Errors and Uncertainties in the Measurement of Ultrasonic Wave Attenuation and Phase Velocity

Alexander N. Kalashnikov, *Member, IEEE* and Richard E. Challis

***Abstract*—This paper presents an analysis of the error generation mechanisms that affect the accuracy of measurements of ultrasonic wave attenuation coefficient and phase velocity as functions of frequency. In the first stage of the analysis we show that electronic system noise, expressed in the frequency domain, maps into errors in the attenuation and the phase velocity spectra in a highly nonlinear way; the condition for minimum error is when the total measured attenuation is around 1 Neper. The maximum measurable total attenuation has a practical limit of around 6 Nepers and the minimum measurable value is around 0.1 Neper. In the second part of the paper we consider electronic noise as the primary source of measurement error; errors in attenuation result from additive noise whereas errors in phase velocity result from both additive noise and system timing jitter. Quantization noise can be neglected if the amplitude of the additive noise is comparable with the quantization step, and coherent averaging is employed. Experimental results are presented which confirm the relationship between electronic noise and measurement errors. The analytical technique is applicable to the design of ultrasonic spectrometers, formal assessment of the accuracy of ultrasonic measurements, and the optimization of signal processing procedures to achieve a specified accuracy.**

I. Introduction

Ultrasonic spectrometers measure the ultrasonic wave attenuation coefficient as a function of frequency, and the more advanced instruments measure wave phase velocity as well, also as a function of frequency. They generally apply to compression waves but similar principles can be employed to measure transverse wave propagation in solid materials. Operating bandwidths vary considerably but generally lie within the 1 MHz to 100 MHz band. The geometrical arrangements of the components in a spectrometer may take many forms. In the simplest case two ultrasonic transducers are aligned coaxially on either side of the test medium contained in a test cell. The test medium can be liquid [1] or solid [2]. The transmission transducer is excited electrically and emits an ultrasonic signal, which passes through the test medium and is received by the receiving transducer. The received signal is amplified and digitized. A signal processing unit, typically a PC or embedded processor, then executes a number of processes on the received data which may include corrections for transducer and field diffraction effects, calibration operations, filtering and/or coherent averaging to improve the signal-to-noise ratio (SNR), and finally calculation of the required functions—attenuation and phase velocity. It is possible to replace the receiving transducer with a plane reflector, a single transducer then acting as both transmitter and receiver—the pulse-echo configuration. The measurement distance (the gauge length) between the transmission transducer and the receiver or reflector is adjustable in the more sophisticated instruments (such as the Ultrasizer, Malvern Instruments Ltd, Malvern, Worcestershire, UK) or may be fixed due to reasons of cost or physical constraints such as in applications to process pipework of predetermined diameter. In all configurations it is important that the active faces of the transducers, or the reflector, be maintained in parallel alignment to avoid signal distortions that ultimately would impose a low pass envelope on the received signal [3].

A typical application of ultrasonic spectrometry to solid materials is the tracking of the cure of epoxy (and other) thermoset materials [4]; here the phase velocity dispersion and the attenuation functions enable the real and imaginary parts of the elastic modulus governing propagation to be tracked during and after the cure of the polymer. Where combined compression and shear wave measurements are used, it is possible to track the separate development of the three principal elasticity parameters—bulk modulus, Young's modulus, and shear modulus [5]. In the case of liquid materials the most common application is in the study of particulate suspensions—solid-in-liquid dispersions and emulsions [6]. The aim of such studies is ultimately to measure the dispersed particle size distribution (the Ultrasizer, mentioned above) and dynamic effects such as flocculation [7] and crystallization [8]. A demanding application is the detection of "no-change" in a reacting material: In an earlier study of a silica sol-gel transition we showed that compression wave phase velocity dispersion remained constant over the transition to within ± 0.01 ms^{-1} over a band between 5 MHz and 45 MHz [9].

In all of the above applications we have observed that our wave propagation data was the least reliable, that is, most variant, in situations where the measured absorption was either very low or very high. This has important implications for the design of process instruments in which it is necessary to optimize the gauge length, the operating

Manuscript received July 15, 2004; accepted February 7, 2005. The authors gratefully acknowledge support for this study from the UK Engineering and Physical Sciences Research Council and the UK Department for Environment, Food and Rural Affairs.

The authors are with the School of Electrical and Electronic Engineering, University of Nottingham, University Park, Nottingham, NG7 2RD, UK (e-mail: alexander.kalashnikov@nottingham.ac.uk).

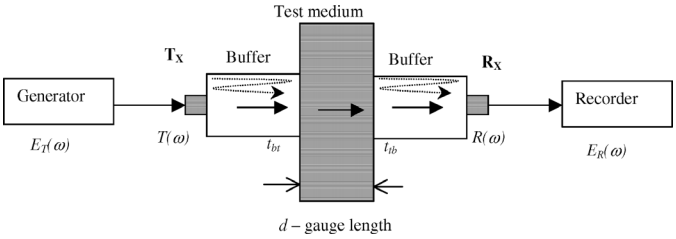

Fig. 1. Basic configuration of an ultrasonic spectrometer. The dotted lines indicate signal paths representing parasitic multiple reflections in the buffers used to couple ultrasound between the transducers and the test medium.

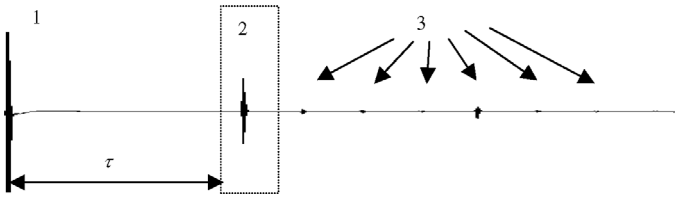

Fig. 2. A typical signal record in the time domain. (1) is the excitation signal breakthrough, (2) is the window of interest, and (3) represents the parasitic multiple reflections. The origin of time ($t = 0$) is the point of transmission, and τ is the time delay to the data acquisition trigger.

frequency range, filtering and averaging schemes to control the SNR, and the design of electronic systems that are crucial to overall spectrometer performance. The principal determinants of errors in measured ultrasonic data are electronic noise (additive, quantization, and timing jitter) and numerical/computational rounding. In this paper we adopt a statistical technique [10] based on Lindley [11] to calculate both variance and bias errors in ultrasonic attenuation and phase velocity in relation to equipment electronic noise. We show that noise maps into measurement errors in a highly nonlinear way and that errors are likely to increase dramatically for both high and low attenuation in the test material, confirming our earlier empirical observations. The analysis provides the basis for optimizing the design of ultrasonic spectrometer systems with applications in both laboratory and process environments.

II. Mapping Variations in Recorded Signals into Uncertainties in Attenuation Coefficient and Phase Velocity

A. Basic Spectrometer Configuration

Fig. 1 shows a schematic of a typical ultrasonic spectrometer. The signal pathway expressed in the frequency domain is

$$S(\omega) = E_T(\omega)E_R(\omega)t_{bt}\,t_{tb}\,T(\omega)\,R(\omega)\,F(\omega)\,X(\omega), \tag{1}$$

where $X(\omega)$ is the response of the test liquid, $E_T(\omega)$ and $E_R(\omega)$ are the frequency responses of the transmitter and receiver electronics, respectively, and $T(\omega)$ and $R(\omega)$ are the responses of the transmission and reception transducers, respectively. The terms t_{bt} and t_{tb} represent the amplitude transmission coefficients between the buffer and the test medium and vice versa, respectively. Nomenclature used in this paper is given in Table I. $F(\omega)$ represents radiation coupling between the transducers and is a function of the acoustic wavenumber in the test liquid and the gauge length d, although it is common to restrict ω to frequencies that approximate near-field coupling conditions, where $F(\omega)$ is assumed to be unity. In a typical operation all of the system-dependent functions are obtained by a calibration using a test liquid with well-known properties, typically distilled, degassed water. Eq. (1) then becomes

$$X(\omega) = S(\omega)/H(\omega). \tag{2}$$

Here we regard $X(\omega)$ as the complex quantity that is apparent from physical measurement, and $H(\omega)$ is the calibration spectrum. In most instruments parasitic multiple reflections will occur in the buffer materials and in the test medium itself, and because of these it is generally advantageous to use a short pulse excitation to the transmitting transducer combined with an appropriate time domain window to select out the first signal component through the test medium (Fig. 2). In any real spectrometer there will be some residual error in the calibration procedure as well as contributions from electronic noise sources—Johnson noise, shot noise, quantization noise, and timing jitter noise. In later sections of this paper we will deal separately with the different types of noise. The ultrasonic propagation variables, attenuation and phase velocity, are related to the true value of $X(\omega)$ which we denote as $\widehat{X}(\omega)$ thus:

$$\widehat{X}(\omega) = \exp\left\{-j\omega\left[\frac{d}{c(\omega)} - \tau\right]\right\}\exp\left[-\alpha(\omega)d\right], \tag{3}$$

where d is the propagation distance in the test medium, $c(\omega)$ is the phase velocity, $\alpha(\omega)$ is the amplitude attenuation coefficient, and τ is the data acquisition delay. The first term gives the signal phase shift referred to the data capture window and includes phase shifts brought about by the frequency-dependent phase velocity, $c(\omega)$. The second term represents amplitude attenuation, again as a function of frequency following Beer's law. Thus, in principle, the phase velocity is calculated from the phase spectrum

$$c(\omega) = \frac{d}{\dfrac{\angle X(\omega)}{\omega} + \tau}, \tag{4}$$

and the attenuation from the amplitude spectrum

$$\alpha(\omega) = -\frac{1}{d}\ln\left|X(\omega)\right|. \tag{5}$$

Due to electronic noise and other errors, the measured spectrum will differ from the true spectrum; we now consider how these errors affect the above two calculations,

TABLE I
NOMENCLATURE.

Operators	*Variables and parameters*	*Indices*
E expectation	$H(\omega)$ calibration spectrum	p phase
F Fourier transform	$S(\omega)$ received spectrum	m modulus (amplitude)
Q quantization	$c(\omega)$ phase velocity	a additive noise
	$\alpha(\omega)$ attenuation coefficient	q quantization noise
Statistical terms	L number of averages	j jitter noise
b bias	N number of data samples in a record	I in-phase component
B relative bias	τ delay between the start of the excitation pulse and start of data acquisition	Q quadrature component
σ standard deviation	r random number with zero mean and unity variance	T true value

and we begin by assuming that the measured spectrum is the sum of the true value, bias in the measured spectrum, and random errors in the measured spectrum, such that

$$\begin{aligned} \left|X(\omega)\right| &= \left|X\right|_T + b_m + r_m\sigma_m \\ \angle X(\omega) &= (\angle X)_T + b_P + r_P\sigma_P \end{aligned}, \tag{6}$$

where the variables b represent measurement bias, r represent random variables with zero mean and unity variance, and σ are the actual standard deviations. In most cases the random variables are expected to be normally distributed. Subscripts T, m, and p relate to the true values, modulus, and phase, respectively. All the variables in the right-hand sides of (6) are functions of frequency, and in subsequent working this dependence will be assumed.

B. Generic Consideration of Bias and Variance

We consider the general case when a required function f is to be calculated from a number of measured variables x_n which are themselves associated with errors in the form of bias and variance. We require estimating the bias and variance in f as functions of the bias and variance associated with measured variables x_n. Following our earlier work [10], [12], [13] we extend the technique of Lindley [11] and expand f about its value, calculated on the basis of means of raw data $\overline{x}_n$ using a Taylor expansion up to second order:

$$\begin{aligned} f(x_0, x_1, \ldots, x_N) &= f(\overline{x}_0, \overline{x}_1, \ldots, \overline{x}_N) \\ &+ \sum_{n=0}^{N} (x_n - \overline{x}_n) \frac{\partial f}{\partial x_n} + \frac{1}{2}\sum_{n=0}^{N} (x_n - \overline{x}_n)^2 \frac{\partial^2 f}{\partial x_n^2} \\ &+ \sum_{n=0}^{N}\sum_{\substack{m=0 \\ m\neq n}}^{N} (x_n - \overline{x}_n)(x_m - \overline{x}_m) \frac{\partial^2 f}{\partial x_n \partial x_m} \\ &+ \text{higher order terms}. \end{aligned} \tag{7}$$

Taking expectations on each side of (7) we obtain f as

$$\begin{aligned} E(f) = f(\overline{x}_0, \overline{x}_1, \ldots, \overline{x}_N) &+ \frac{1}{2}\sum_{n=0}^{N} \sigma_n^2 \frac{\partial^2 f}{\partial x_n^2} \\ &+ \sum_{n=0}^{N}\sum_{\substack{m=0 \\ m\neq n}}^{N} \rho_{nm}\sigma_n\sigma_m \frac{\partial^2 f}{\partial x_n \partial x_m}, \end{aligned} \tag{8}$$

where σ_n is the variance of x_n, and ρ_{nm} is the correlation coefficient of x_n on x_m. If each $\overline{x}_n$ is associated with a bias b_n with respect to its true value x_n^T,

$$b_n = \left(\overline{x} - x_n^T\right); \tag{9}$$

then the bias in f becomes

$$\begin{aligned} b(f) &= E\left(f\left(x_0, x_1, \ldots, x_N\right)\right) - f\left(x_0^T, x_1^T, \ldots, x_N^T\right) \\ &= \sum_{n=0}^{N}\left(b_n \frac{\partial f}{\partial x_n} + \frac{1}{2}\sigma_n^2 \frac{\partial^2 f}{\partial x_n^2}\right) \\ &+ \sum_{n=0}^{N}\sum_{\substack{m=0 \\ m\neq n}}^{N} \rho_{nm}\sigma_n\sigma_m \frac{\partial^2 f}{\partial x_n \partial x_m}. \end{aligned} \tag{10}$$

The variance in f is obtained by taking the variance of the right-hand side of (7), approximated to first order:

$$\sigma_f^2 = \sum_{n=0}^{N} \sigma_n^2 \left(\frac{\partial f}{\partial x_n}\right)^2 + 2\sum_{n=0}^{N}\sum_{\substack{m=0 \\ m\neq n}}^{N} \rho_{nm}\sigma_n\sigma_m \frac{\partial^2 f}{\partial x_n \partial x_m}. \tag{11}$$

It is useful to consider relative bias and relative standard deviation by dividing (10) and (11) by some notional true value and expressing the result as a percentage error. However, the true value $f\left(x_n^T\right)$ will be the subject of measurement and not known *a priori*, and so expected values $E\left(f\left(x_n\right)\right)$ are used to give estimates of relative errors.

C. Errors in the Estimate of Attenuation Coefficient $\alpha(\omega)$

The attenuation coefficient is calculated from a spectrum $X(\omega)$ measured over a distance d following (5). The bias in $\alpha(\omega)$ according to (10) is

$$\begin{aligned} b[\alpha(\omega)] = b(d)\frac{\partial \alpha(\omega)}{\partial d} &+ b_m \frac{\partial \alpha(\omega)}{\partial \left|X(\omega)\right|} \\ &+ \frac{1}{2}\sigma^2(d)\frac{\partial^2 \alpha(\omega)}{\partial d^2} + \frac{1}{2}\sigma_m^2 \frac{\partial^2 \alpha(\omega)}{\partial \left|X(\omega)\right|^2}. \end{aligned} \tag{12}$$

Here we assume that there is no correlation between $\alpha(\omega)$ and d and so the summation term for $n \neq m$ in (10) is zero. Taking (12) term by term we get

$$\begin{aligned}\frac{\partial\alpha(\omega)}{\partial d} &= \frac{\ln\left|X(\omega)\right|}{d^2};\\ \frac{\partial\alpha(\omega)}{\partial\left|X(\omega)\right|} &= -\frac{1}{\left|X(\omega)\right|}\frac{1}{d};\\ \frac{\partial^2\alpha(\omega)}{\partial d^2} &= -\frac{2\ln\left|X(\omega)\right|}{d^3};\\ \frac{\partial^2\alpha(\omega)}{\partial\left|X(\omega)\right|^2} &= \frac{1}{\left|X(\omega)\right|^2}\frac{1}{d}.\end{aligned} \tag{13}$$

If we approximate the notional true value of $\alpha(\omega)$ by (5), the relative bias in $\alpha(\omega)$ becomes

$$\begin{aligned}B[\alpha(\omega)] = &-b(d)\frac{\ln\left|X(\omega)\right|}{d^2}\frac{d}{\ln\left|X(\omega)\right|}\\ &+ b_m\frac{(-1)}{\left|X(\omega)\right|d}\cdot\frac{-d}{\ln\left|X(\omega)\right|}\\ &+ \frac{1}{2}\sigma^2(d)\left(-2\frac{\ln\left|X(\omega)\right|}{d^3}\right)\cdot\frac{-d}{\ln\left|X(\omega)\right|}\\ &+ \frac{1}{2}\sigma^2(|X(\omega)|)\frac{l}{\left|X^2(\omega)\right|d}\cdot\frac{-d}{\ln\left|X(\omega)\right|},\end{aligned} \tag{14}$$

or

$$\begin{aligned}B[\alpha(\omega)] = &-\frac{b(d)}{d} + \frac{b_m}{\left|X(\omega)\right|}\cdot\frac{1}{\ln\left|X(\omega)\right|}\\ &+ \frac{\sigma^2(d)}{d^2} - \frac{1}{2}\frac{\sigma_m^2}{\left|X^2(\omega)\right|}\cdot\frac{1}{\ln\left|X(\omega)\right|}.\end{aligned}$$

We now substitute for $|X(\omega)|$ from (5), and the second and fourth terms in (14) become, respectively,

$$B_2(\alpha(\omega)) = \frac{-b_m}{\alpha(\omega)de^{-\alpha(\omega)d}}; \tag{15}$$

$$B_4(\alpha(\omega)) = \frac{\sigma_m^2}{2\alpha(\omega)d\,e^{-2\alpha(\omega)d}}. \tag{16}$$

From (15) we see that the original bias in $|X(\omega)|$ contributes to the relative bias in the measured $\alpha(\omega)$ by the factor

$$M_m(x) = \frac{\exp(x)}{x}, \tag{17}$$

where $x = \alpha(\omega)d$, the actual measured attenuation expressed in Nepers. Similarly, the variance term contributes to B_4 in (16) by the factor $M_m(z)$, where $z = 2\alpha(\omega)d$. We can rewrite (15) and (16) in the following form:

$$B_2(\alpha(\omega)) = -b_m M_m[\alpha(\omega)d]; \tag{18}$$

$$B_4(\alpha(\omega)) = \sigma_m^2 M_m[2\alpha(\omega)d]. \tag{19}$$

M_m is a magnification factor which expresses the mapping of errors in the raw data domain into the domain of measured variables; it exhibits a minimum value $e = 2.718$ when $x = 1$. The contribution of (18) is minimized when the total measured attenuation is $\alpha(\omega)d = 1$ Neper. The contribution of (19) is minimized when $\alpha(\omega)d = 0.5$ Neper. The functions $M_m[\alpha(\omega)d] = M_1$ and $M_m[2\alpha(\omega)d] = M_2$ are shown plotted in Fig. 3. We note the abrupt increases in both functions for low and high values of measured attenuation, and in a later section of this paper we consider the implications of this in relation to the practical limits for measurement.

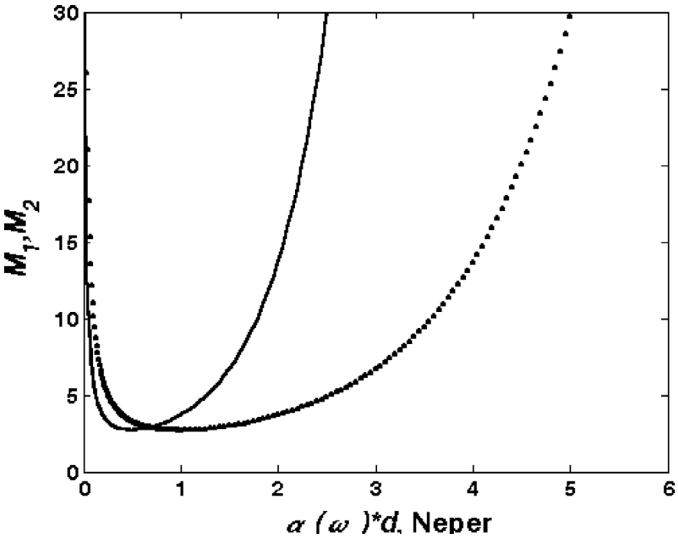

Fig. 3. The magnification functions M_2 (solid line) and M_1 (dotted line) versus total attenuation expressed in Nepers.

The derivation of the variance in the measured attenuation is based on (11) with the correlation terms set to zero as before. The variance in $\alpha(\omega)$ normalized to $\alpha^2(\omega)$ becomes

$$\frac{\sigma^2(\alpha(\omega))}{\alpha^2(\omega)} = \frac{\sigma^2(d)}{d^2} + \frac{\sigma_m^2}{\left|X^2(\omega)\right|}\cdot\frac{1}{\left(\ln\left|X(\omega)\right|\right)^2}. \tag{20}$$

The first term reflects the uncertainty in measurement distance d. We interpret the second term as before, and setting $\left|X(\omega)\right| = e^{-\alpha(\omega)d}$ from (5),

$$\begin{aligned}\frac{\sigma^2(\alpha(\omega))}{\alpha^2(\omega)} &= \frac{\sigma^2(d)}{d^2} + \frac{\sigma_m^2}{\left(\alpha(\omega)d\,e^{-\alpha(\omega)d}\right)^2}\\ &= \frac{\sigma^2(d)}{d^2} + \sigma_m^2 M_m^2[\alpha(\omega)d].\end{aligned} \tag{21}$$

In a manner similar to that for bias in $\alpha(\omega)$, the effect of the system noise is magnified by a factor $M_m^2[\alpha(\omega)d]$ to get its contributions to the relative variance in $\alpha(\omega)$. This factor has a minimum value of $e^2 = 7.39$ when the measured attenuation is 1 Neper.

D. Errors in the Estimate of the Phase Velocity $c(\omega)$

The ultrasonic phase velocity is obtained from the phase spectrum $\phi(\omega) = \angle X(\omega)$, (4). The bias in $c(\omega)$ according to (10) is

$$b[\alpha(\omega)] = b(d)\frac{\partial c(\omega)}{\partial d} + b_P \frac{\partial c(\omega)}{\partial\left(\angle X(\omega)\right)} + \frac{1}{2}\sigma^2(d)\frac{\partial^2 c(\omega)}{\partial d^2} + \frac{1}{2}\sigma_p^2 \frac{\partial^2 c(\omega)}{\partial\left(\angle X(\omega)\right)^2}. \quad (22)$$

Here we again assume that there is no correlation between $\alpha(\omega)$ and d and so the summation term for $n \neq m$ in (10) is zero. Taking (12) term by term we get

$$\begin{aligned} \frac{\partial c(\omega)}{\partial d} &= \frac{c}{d}; \\ \frac{\partial c(\omega)}{\partial\left(\angle X(\omega)\right)} &= -\frac{c^2}{\omega d}; \\ \frac{\partial^2 c(\omega)}{\partial d^2} &= \frac{c}{d^2}; \\ \frac{\partial^2 c(\omega)}{\partial\left(\angle X(\omega)\right)^2} &= 2\frac{c^3}{(\omega d)^2}. \end{aligned} \quad (23)$$

Then the relative bias becomes

$$B[c(\omega)] = \frac{b(d)}{d} - b_p \frac{c}{\omega d} + \sigma_p^2 \left(\frac{c}{\omega d}\right)^2 + \frac{1}{2}\frac{\sigma^2(d)}{d^2}. \quad (24)$$

By denoting the magnification term

$$M_p = \frac{c}{\omega d}, \quad (25)$$

the relative bias becomes

$$B[c(\omega)] = \frac{b(d)}{d} - b_p M_p + \sigma_p^2 M_p^2 + \frac{1}{2}\frac{\sigma^2(d)}{d^2}. \quad (26)$$

This result is in line with expectation on the basis of physical intuition; relative errors increase for high measured phase velocities and decrease as the gauge length is increased. The derivation of the variance in the measured phase velocity is based on (11) with the correlation terms set to zero as before. The variance in $c(\omega)$ normalized to $c^2(\omega)$ becomes

$$\frac{\sigma^2(c(\omega))}{c^2(\omega)} = \frac{\sigma^2(d)}{d^2} + \sigma_p^2 M_p^2. \quad (27)$$

Again we see that errors increase with measured phase velocity and decrease with longer gauge lengths. More generally it will be noted that gauge length d appears in (14), (21), (24), and (27), either because it contributes to total attenuation or because it affects velocity measurement. The *variance* of the gauge length has an effect only if the gauge length is changing. In situations where gauge length itself is fixed for some reason, it will still affect the frequency range within which $\alpha(\omega)$ and $c(\omega)$ are measurable within acceptable limits of error. The results obtained so far are summarized in Table II; we now focus on the effects on measurement errors of system-generated noise and the statistical properties of received signals.

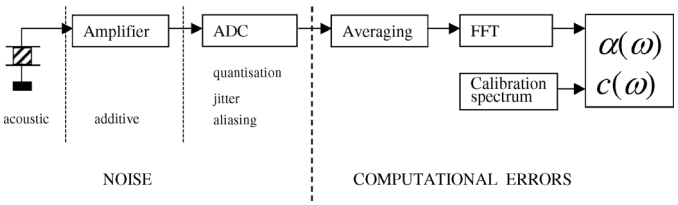

Fig. 4. Typical signal processing chain showing associated errors.

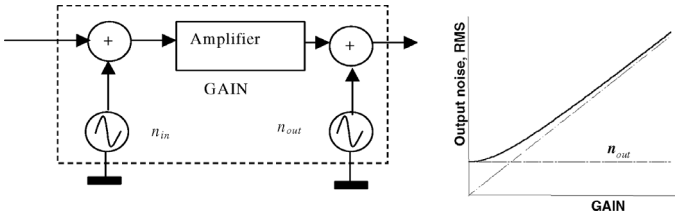

Fig. 5. Noise model for a typical receiver amplifier: (a) schematic diagram, and (b) RMS noise level at the output versus gain.

III. The Effects of Electronic Noise and Signal Processing

We now consider how electronic noise maps into uncertainties in the measured amplitude spectra and thence affects errors in the estimation of $\alpha(\omega)$ and $c(\omega)$.

A. Basic Signal Processing Scheme

Fig. 4 shows a typical system for the acquisition and processing of acoustic spectroscopy signals. The figure includes acoustic noise at the input of the system to represent parasitic multiple reflections, which are generally eliminated by careful choice of the data capture window (Fig. 2); this noise will not be considered further in this paper. Additive noise is inherent in all analogue electronic devices, and a typical system can be modeled according to Fig. 5. Two noise sources are shown: n_{out} is independent of the gain setting of the amplifier, and n_{in}, is an effective input noise component and is amplified; the influence of the latter on the system therefore depends on gain G. The net additive noise at the amplifier output is thus $\sqrt{(n_{in}G)^2 + n_{out}^2}$; its distribution in frequency can be either uniform (white noise) or nonuniform (colored noise). The setting of the gain of the amplifier should be such as to maximize the SNR and to make optimum use of the dynamic range of the analogue-to-digital converter (ADC), leaving some headroom to avoid saturation.

The phenomenon of *aliasing* inevitably occurs when analog signals are converted into digital form. As a source of data errors it can be treated as a form of noise that ultimately affects the overall system SNR. The severity of the effects of this noise depends on the bandwidth of the signal compared to the sampling frequency. It can be quantified [14] as a relative aliasing error e_{al}:

$$e_{al} \leq 9.5\left(\Delta f / f_s\right)^2, \quad (28)$$

TABLE II
RESULTS OF PRELIMINARY STATISTICAL ANALYSIS.

	Attenuation coefficient	Phase velocity
Relative bias	$B[\alpha(\omega)] = -b_m M_m[\alpha(\omega)d] + \sigma_m^2 M_m[2\alpha(\omega)d]$	$B[c(\omega)] = -b_p M_p + \sigma_p^2 M_p^2$
Relative variance	$\frac{\sigma^2(\alpha(\omega))}{\alpha^2(\omega)} = \sigma_m^2 M_m^2[\alpha(\omega)d]$	$\frac{\sigma^2(c(\omega))}{c^2(\omega)} = \sigma_p^2 M_p^2$
Magnifying factor	$M_m(x) = \frac{\exp(x)}{x}$	$M_p = \frac{c}{\omega d}$

where Δf is the system bandwidth and f_s is the sampling frequency. For typical acoustic spectroscopy systems e_{al} can often be neglected; for example, a typical arrangement based on a 10-MHz transducer with a bandwidth of 60% of the center frequency and a sampling frequency of 400 MHz results in e_{al} around 0.2%, which is negligible compared to other sources of error. However, if the sampling frequency is reduced to its lower practical limit, 40 MHz for the 10-MHz transducers, then e_{al} will rise to around 20%, which cannot be neglected. *Quantization noise* occurs in the ADC and arises from the expression of continuous signals with a continuous range of amplitudes in digital form with a finite number of binary bits. *Jitter noise* arises from random timing errors during the signal sampling process. In most systems ultrasonic data are digitized in frames of, typically, 1024 or 2048 samples, and jitter can occur in the timing of the start of the frame or in the intervals between individual samples within a given frame. In practice we have found that frame jitter is the dominant source of error, whereas individual sample jitter can be neglected. *Coherent averaging* of successive frames is usually necessary to improve the SNR; L averages give an improvement in the SNR of $\sqrt{L}$. In principle the averaging process could be associated with arithmetic rounding errors, but if floating point arithmetic is used, such errors are negligible. However, frame jitter does impinge upon coherent averaging, and we shall discuss the implication of this later. *Frequency transformation* by fast Fourier transform (FFT) involves significant computation with associated numerical errors, although if, as is usual, floating point arithmetic is employed with a resolution of at least 20 bits, these errors are negligible [15]. The final calculations of $\alpha(\omega)$ and $c(\omega)$ are potentially ill-conditioned and consequently are usually carried out using double-precision arithmetic; this renders computational errors insignificant. Consequently the equation for the evaluation of the frequency spectrum of the recorded pulse becomes

$$S(\omega) = F\left\{\frac{1}{L}\sum_{l=1}^{L} Q\left[s\left(t-\Delta t_l\right)+n_l\right]\right\}, \qquad (29)$$

where Q is a quantization operator, F is the Fourier transform operator, s is the true signal, n_l represents the additive noise, and Δt_l represents the effect of the frame jitter. We now consider the effects of quantization, additive noise, and timing jitter.

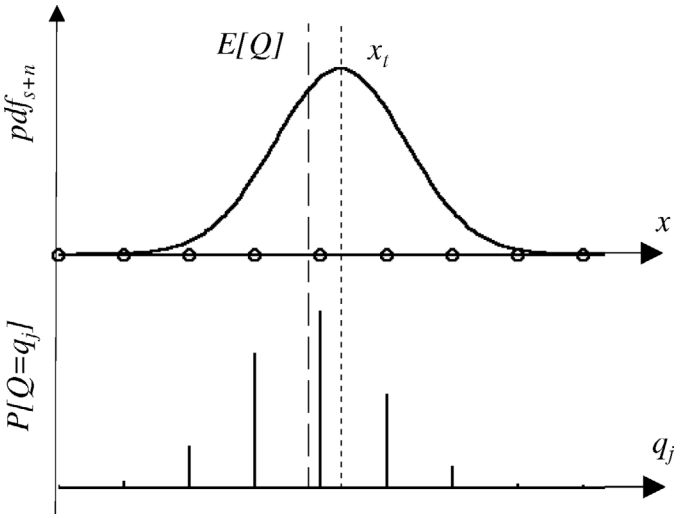

Fig. 6. Continuous PDF of the mixture signal plus noise (above) that transforms by digitization into a discrete probability mass function (below). Quantization levels are shown by circles. The dotted line represents the true value, and the dashed line represents the expected value.

B. The Influence of Quantization

Fig. 6 shows the amplitude distribution of additive noise centered on the notional true signal value s at time t ($x_t = s(t)$). The horizontal axis is calibrated in quantization amplitude steps q_j, q_{j+1}, etc. The quantized amplitude is a discrete random variable $Q = q_j$. When the signal is quantized, there will exist the probability $P(Q = q_j)$ that the quantized value will be q_j:

$$P(Q = q_j) = \int_{q_j}^{q_{j+1}} pdf_{s+n}(x)dx, \qquad (30)$$

where n is the noise amplitude at t, pdf_{s+n} is the probability density function (PDF) of the signal and noise mixture at the same t. L successive measurements will result in obtaining L values Q_l with the average value of

$$Q_L = \sum_{l=1}^{L} Q_l. \qquad (31)$$

Due to quantization and the finite value of L, this value could be different from the expected value

$$E[Q] = \sum_{l} P(Q = q_l)q_l, \qquad (32)$$

shown by the vertical dashed line in Fig. 6. Thus the bias in the digitized value is

$$b(x_t) = x_t - E[Q]. \tag{33}$$

The variance of Q for L averaged measurements is

$$\sigma^2(Q_L) = \frac{1}{L}\sum_{l=1}^{L}\{Q_l - Q_L\}^2 \approx \frac{1}{L}\left\{\sum_l P(Q=q_l)q_l^2 - E^2[Q]\right\}, \tag{34}$$

where the right-hand part represents the expected value at high values of L. After L averages, the digitized datum is the random variable

$$x_r = E[Q] + r_1\sigma(Q_L) = x_t + b + r_1\sigma(Q_L), \tag{35}$$

where r_1 is a random variable whose PDF is of the same form as that of Q but which has zero mean and unity variance. In the above, b and r_1 are associated with digitization at a given time t in the signal record; they both depend on the difference between x, and the nearest quantization value q_j on the left-hand side of x_t (see Fig. 6). Following [16]–[18] the difference $x_t - q_j$ is considered as a random variable uniformly distributed between q_j and q_{j+1}, the quantization box. We obtain

$$x_r = x_t + \overline{b} + r_1\sqrt{\overline{\sigma_q^2}} + r_2\sqrt{\left(b-\overline{b}\right)^2}. \tag{36}$$

The bars over the variables represent averages taken over the quantization box, and the random variable r_2 has unity variance and represents the PDF of the bias. A simple simulation has been used to investigate the effects of the last two terms in (36). The additive noise was assumed to be Gaussian with the ratio of the standard deviation σ_a to the quantization step varied up to a maximum of 80 dB. The quantization box was divided into 10,000 equal intervals, and at the center of each, b and σ_q were calculated using (32)–(34); these values were then averaged over the quantization box to evaluate the variance and bias terms in (36). As expected, the average bias remained constant at $-0.5q$ for all noise levels. Fig. 7 shows the ratio of the calculated variance $\sqrt{\overline{\sigma_q^2}}$ divided by the quantization step q plotted against σ_a, again divided by the quantization step q. Two asymptotes are shown on the figure. The horizontal dashed line represents the standard deviation of the quantization noise with a value $q/\sqrt{12}$, and the second asymptote represents the additive noise *per se* and has a slope of unity. The X's on the figure represent the calculated results. It is clear that for $\sigma_a/q > 0.2$ the variance term can be approximated by

$$\sigma_q^2 \approx \sigma_a^2 + q^2/12. \tag{37}$$

The region $\sigma_a/q > 0.2$ in (37) provides a set of maximum values related to the quantization noise, and can be used as an upper estimate for the cumulative (additive and quantization) noise without the need of extensive simulation; the solid line in Fig. 7 represents this approximation. Thus the impact of quantization noise on the averaged noise after digitizing is small relative to the additive noise; this is in agreement with the earlier results of Brown [19]. Fig. 8 shows the results for the final (bias) term in (36). For low amplitudes of additive noise, $\sqrt{\overline{(b-\overline{b})^2}}$ approaches $q/\sqrt{12}$; for additive noise of the order of or greater than the quantization step, the bias term approaches zero. Thus if the additive noise amplitude exceeds the quantization step and if floating point averaging arithmetic is used, then the influence of quantization is negligible. Finally, we can take the combined quantization and frequency transformation without including the quantization operator:

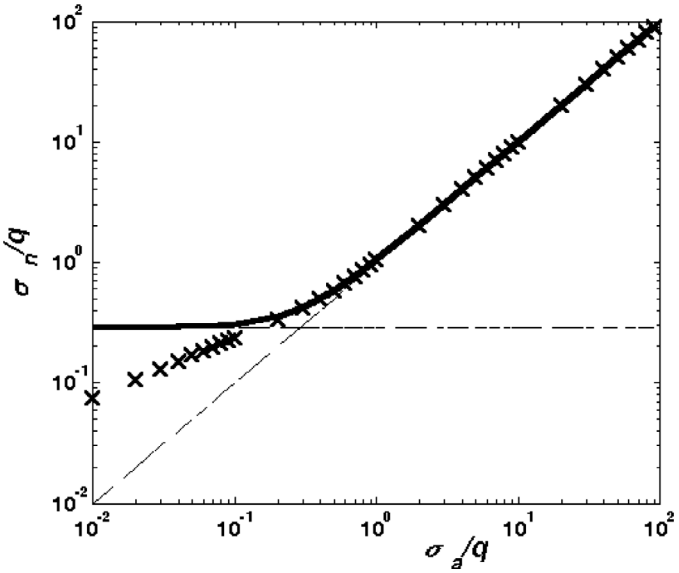

Fig. 7. Standard deviation of additive noise after quantization versus the standard deviation of the additive noise itself, both normalized to the quantization step q (X's). The horizontal asymptote represents the quantization noise itself, and the sloped asymptote the additive noise in the absence of quantization. The solid line represents approximation (37).

$$S(\omega) \approx \frac{1}{L}F\left\{\sum_{l=1}^{L}x(t-\Delta t_l)\right\} + \frac{1}{L}F\left\{\sum_{l=1}^{L}n_l\right\}. \tag{38}$$

C. The Influence of Additive Noise

The last term in (34) represents the discrete Fourier transformation of additive noise in the time domain. Following earlier considerations by Schoukens and Renneboog [20] and by Blair [14] we can represent this term as

$$\frac{1}{L}F\left\{\sum_{l=1}^{L}n_1\right\} \approx r_3\sigma_a\sqrt{\frac{N}{2L}} + jr_4\sigma_a\sqrt{\frac{N}{2L}}, \tag{39}$$

where r_3 and r_4 are uncorrelated random variables of zero mean and unity variance, and σ_a is the noise standard

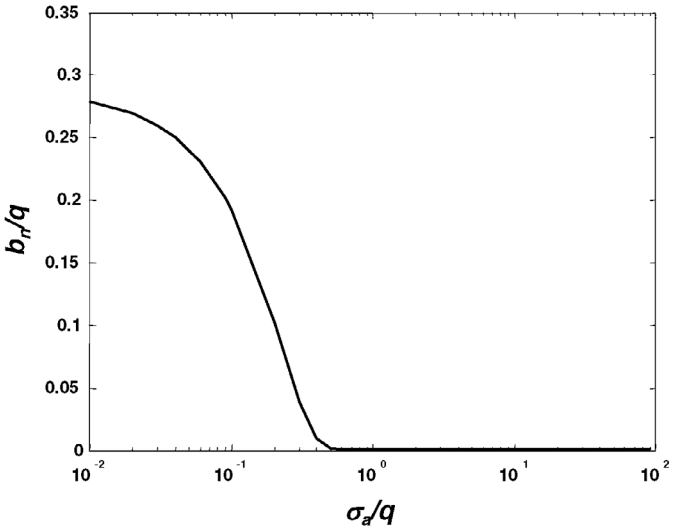

Fig. 8. Bias b_n induced by the additive noise versus the standard deviation of the additive noise, both normalized to the quantization step q.

deviation. N is the number of data samples in the transformation and L is the number of coherent averages. The divisor 2 in the two terms on the right-hand side of (39) arises from an equal partition of the noise power into the real and imaginary parts of the transformation. The expression holds for spectrally white noise but a correction is required when the noise is band-limited [20]. For example, if the sampling system operates at a rate of 400 MHz and the noise is band-limited to 100 MHz, then σ_n would be increased by a factor of $\sqrt{2}$ up to 100 MHz and set to zero thereafter. In general, σ_a should be considered as a function of frequency $\sigma_a(\omega)$. It is apparent from (39) that in order to achieve a given frequency resolution by setting the time domain record length, it would be better to pad the received signal record with zeroes rather than to record larger numbers of actual data samples.

D. The Influence of Timing Jitter

The variable Δt_l represents jitter in (29). If we assume that Δt_l is relatively small and that we are concerned with frequencies much less than the sampling frequency, we get:

$$\frac{1}{L}F\left\{\sum_{l=1}^{L}s(t-\Delta t_l)\right\}=\frac{1}{L}\sum_{l=1}^{L}F\left\{s(t)\right\}\exp(j\omega\Delta t_l). \tag{40}$$

For $\omega\Delta t_l \ll 1$, the exponential term approximates to

$$\omega\Delta t_l \ll 1 \;\;\Rightarrow\;\; \exp(j\omega\Delta t_l)\approx 1+j\omega\Delta t_l, \tag{41}$$

from whence (40) becomes

$$\frac{1}{L}\sum_{l=1}^{L}F\left\{s(t-\Delta t_l)\right\}=F\left\{s(t)\right\}+F\left\{s(t)\right\}\frac{j\omega}{L}\sum_{l=1}^{L}\Delta t_l. \tag{42}$$

The first term on the right-hand side of (42) represents the undisturbed signal spectrum $S_T(\omega)$; the second term is proportional to the sum of Δt_l which can be considered as a random variable with zero mean and standard deviation σ_j. Eq. (40) can therefore be written as

$$\frac{l}{L}F\left\{\sum_{l=1}^{L}s(t-\Delta t_l)\right\}\approx S_T(\omega)+\frac{j\omega}{\sqrt{L}}S_T(\omega)\sigma_j r_5, \tag{43}$$

where r_5 has zero mean and unity variance and a form that corresponds to the jitter PDF which is generally taken as Gaussian [14], [21].

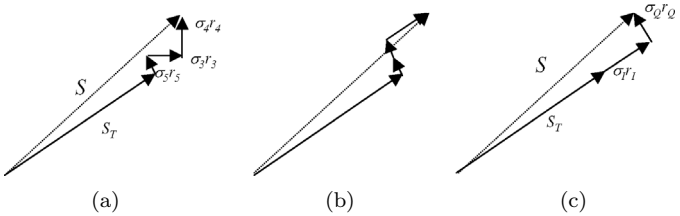

Fig. 9. Phasor diagrams of the spectral estimate S: (a) following (44), (b) after rotation of the additive noise components, and (c) following (45).

E. The Influence of Electronic Noise from All Sources

Combining (39) and (43) we get

$$S(\omega)=$$
$$S_T(\omega)+\frac{j\omega}{\sqrt{L}}S_T(\omega)\sigma_j r_5+r_3\sigma_a\sqrt{\frac{N}{2L}}+jr_4\sigma_a\sqrt{\frac{N}{2L}}. \tag{44}$$

Thus the spectrum estimated from an averaged record depends on three random vectors on the phasor diagram that is shown in Fig. 9(a). The orthogonal components representing the additive noise can be rotated on the diagram by an arbitrary angle [14], and we can therefore set one component in phase with S_T, and a second one in quadrature to S_T [Fig. 9(b)]. This reduces the noise components to simple in-phase and quadrature components [Fig. 9(c)]; (44) becomes:

$$S(\omega)=\frac{S_T(\omega)}{\left|S_T(\omega)\right|}\left(\left|S_T(\omega)\right|+\sigma_I r_I+j\sigma_Q r_Q\right), \tag{45}$$

where

$$\sigma_I^2=\sigma_a^2\frac{N}{2L};\;\;\sigma_Q^2=\sigma_a^2\frac{N}{2L}+\sigma_j^2\frac{\left|S_T\right|^2\omega^2}{L}. \tag{46}$$

If the averaged signal possesses a reasonable SNR, that is, $\left|S_T\right| \gg \sigma_I$ and $\left|S_T\right| \gg \sigma_Q$, we can obtain the statistical parameters of the amplitude and phase spectra:

$$|S|=\sqrt{\left(\left|S_T\right|+\sigma_I r_I\right)^2+\left(\sigma_Q r_Q\right)^2}\approx\left|S_T\right|+\sigma_I r_I, \tag{47}$$

$$\angle X-\angle X_T=\angle S-\angle S_T=$$
$$\arctan\frac{\sigma_Q r_Q}{\left|S_T\right|+\sigma_I r_I}\approx\frac{\sigma_Q r_Q}{\left|S_T\right|}, \tag{48}$$

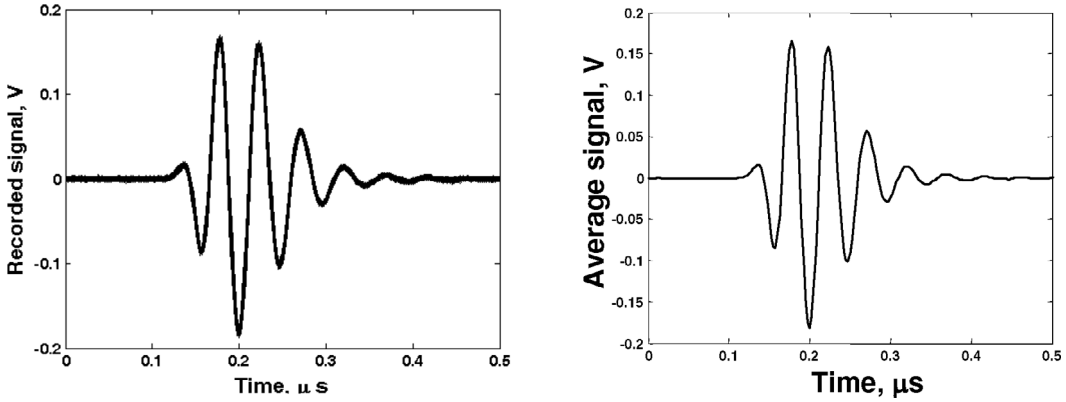

(a) (b)

Fig. 10. Recorded signals: (a) superimposed in the time domain, and (b) after coherent averaging.

from which

$$E\{|S|\} = |S_T|; \;\; E\{|X|\} = \frac{|S_T|}{|H|}; \;\; b_m = 0;$$
$$\sigma_m(\omega) = \frac{\sigma_I(\omega)}{|H|} = \frac{\sigma_a(\omega)}{|H|}\sqrt{\frac{N}{2L}} \tag{49}$$

and

$$E\{\angle X\} = \angle S_T - \angle H; \;\; b_p = 0;$$
$$\sigma_p(\omega) = \sqrt{\frac{\sigma_a^2(\omega)}{|S_T|^2}\frac{N}{2L} + \sigma_j^2\frac{\omega^2}{L}}. \tag{50}$$

Consequently, electronic noise introduces no bias in the amplitude and phase spectra of the received signal. The frame jitter noise affects only the phase spectrum, whereas the additive noise affects both amplitude and phase spectra (see Table III).

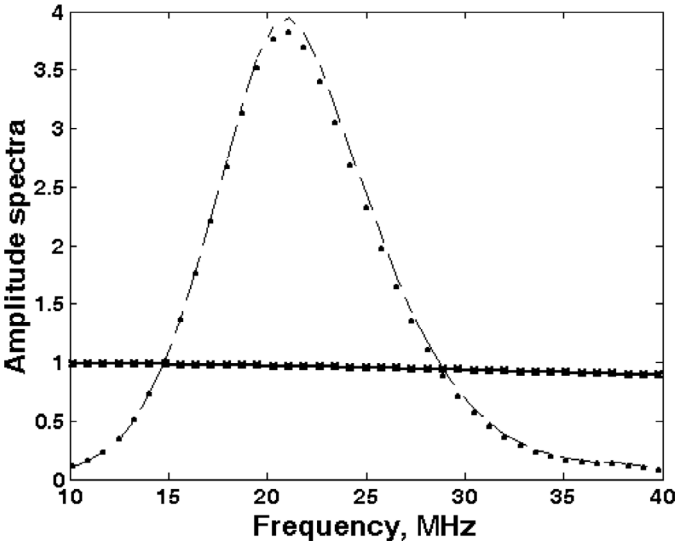

Fig. 11. Frequency domain results for water: Theoretical propagation loss (solid line with X's), averaged amplitude spectrum $|S_T(\omega)|$ (dotted line), and the derived calibration spectrum $|H(\omega)|$ (dashed line).

IV. Verifying Experiments and Results

Experimental data were collected using a commercial ultrasonic pulser-receiver with an operating bandwidth of 60 MHz (UPR, NDT Solutions Ltd, Chesterfield, UK); received and amplified data were recorded using a digital storage oscilloscope (DSO, model 9450, LeCroy Inc., Chestnut Ridge, NY), sampling at 400 MHz. The ultrasonic transducers (V317, Panametrics Inc., Waltham, MA) had a center frequency of 20 MHz and a bandwidth around 14 MHz. The test medium was chosen to be water because its properties are well documented; the ultrasonic path length in the water was set to $d = 3.2$ mm. Data consisting of 1000 frames of 202 samples each were collected with the trigger delay set to $\tau = 2$ μs. The raw signal records [Fig. 10(a)] exhibit noticeable noise that is significantly reduced by coherent averaging [Fig. 10(b)]. The Fourier transform of every record was calculated, and the amplitude and phase spectra were averaged separately. These averaged spectra were regarded as true received spectra $|S_T(\omega)|$ and $\angle S_T(\omega)$, respectively. Water was considered in all practical senses as a dispersion-free medium obeying Beer's law [22] with the attenuation coefficient

$$\alpha_T(\omega) = 2.3(f/10\ \text{MHz})^2 \;\; [\text{Neper/m}]. \tag{51}$$

The calibration amplitude spectrum was derived as

$$|H(\omega)| = \frac{|S_T(\omega)|}{\exp(-\alpha_T(\omega)d)}. \tag{52}$$

The theoretical attenuation, averaged amplitude spectrum, and calculated calibration spectrum are shown in Fig. 11. The phase spectrum was unwrapped within the range 10–40 MHz, and a least squares linear fit was applied in order to determine its gradient [23]. The value obtained was 1.15 rad/MHz, and hence the theoretical phase spectrum was

$$\varphi(\omega) = 1.15(f/\text{MHz}) \;\; [\text{rad}], \tag{53}$$

TABLE III
EFFECTS OF INSTRUMENTATION NOISE ON AMPLITUDE AND PHASE SPECTRA.

	Bias induced by the instrumentation noise	Standard deviation induced by the instrumentation noise
Amplitude spectrum	$b_m = 0$	$\sigma_m(\omega) = \frac{\sigma_a(\omega)}{\lvert H\rvert}\sqrt{\frac{N}{2L}}$
Phase spectrum	$b_p = 0$	$\sigma_p(\omega) = \sqrt{\frac{\sigma_a^2(\omega)}{\lvert S_T\rvert^2}\frac{N}{2L} + \sigma_j^2\frac{\omega^2}{L}}$

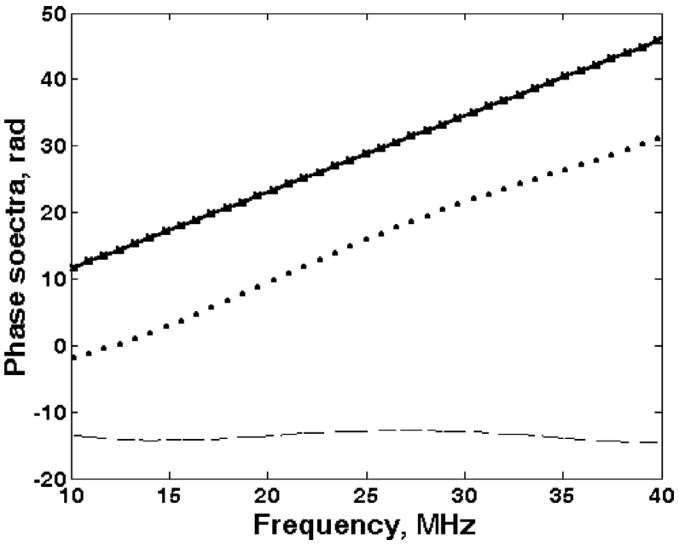

Fig. 12. Frequency domain results for water: Theoretical phase spectrum (solid line with X's), averaged phase spectrum $\angle S_T(\omega)$ (dotted line), and the derived calibration spectrum $\angle H(\omega)$ (dashed line).

and the calibration phase spectrum

$$\angle H(\omega) = \angle S_T(\omega) - \varphi(\omega). \tag{54}$$

These spectra are shown in Fig. 12. The additive noise was quantified by calculation of the standard deviation of the amplitude spectrum [Fig. 13(a)], equal to $\sigma_a(\omega)\sqrt{N/2}$. By relating this to $\lvert S_T(\omega)\rvert$ we obtained an SNR greater than 20 dB in the range of 10–37 MHz and greater than 40 dB in the range of 17–27 MHz [Fig. 13(b)]. The standard deviation of the phase spectrum was obtained from the experimental records and compared to the curve obtained using (50) with $\sigma_j = 0.72$ ns; Fig. 14 shows good agreement between these two results.

Finally, the attenuation coefficient and phase velocity were calculated for each of the unaveraged records. Fig. 15 shows the attenuation results superimposed on the theoretical curve; it is clear that the experimental data are highly variant, particularly at the low- and high-frequency ends of the spectrum. This illustrates the effect of the gauge length (d) and magnification function (M_m) terms on the right-hand side of (21). This is illustrated further in Figs. 16 and 17 where the experimental relative bias and standard deviations are plotted together with theoretical values calculated using Table I. The calculated theoretical data were obtained using measured additive noise spectra rather than a Gaussian approximation to idealized white noise [13], and an excellent match can be seen between the two curves. Equivalent data for the phase velocity, its relative bias, and its standard deviation are shown on Figs. 18 to 20, from which it can be seen that there is, again, excellent agreement between measured and theoretical results.

V. Discussion

The considerations above have shown that the principal effect of electronic noise is to impart variance to measured attenuation and phase velocity data, and that any bias in measured data, which results from noise, is negligible. We now consider the implications of these results for the calibration of ultrasonic instruments, and the estimation of measurement uncertainty—both for one-shot recordings and when a number of records are coherently averaged.

A. Instrument Calibration

Ultrasonic spectrometers require calibration procedures that essentially determine the frequency response and gain of the electronic system, and the frequency response and the insertion loss of the transmitting and receiving transducers and the coupling layers with which they are linked to the test medium proper. In order to estimate the *statistical* performance of the system and to plan noise reduction strategies such as filtering and coherent averaging, it is also necessary to determine the additive and jitter noise properties of the system. The additive noise is best measured as a number of frames of data with the electronics connected to the transducers but with the output of the transmitter pulser switched off. The statistics of the frame jitter are more difficult to assess, and in an earlier publication [24] we have suggested a dedicated algorithm that can be used to make reliable estimates of the standard deviation of the jitter. The key to the method is to first estimate the standard deviation of the received phase spectrum as a function of angular frequency and then to fit a straight line to the data using the least mean squares method. The slope of the line gives the required standard deviation directly. The method requires no special experimental conditions and can easily be combined with other calibration procedures. In many experiments on a number of different systems from various manufacturers, we have

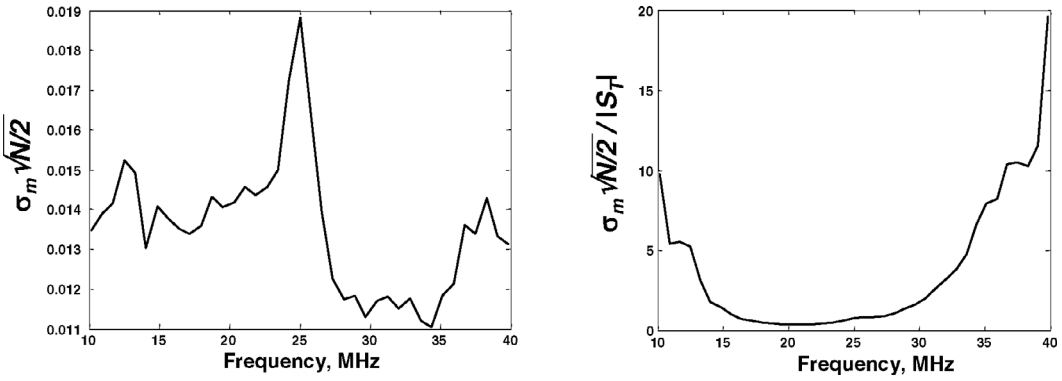

(a) (b)

Fig. 13. Standard deviation of the measured amplitude spectrum $\sigma_m(\omega)\sqrt{N/2}$: (a) absolute value, and (b) normalized to the averaged spectral values $\left|S_T(\omega)\right|$ expressed as a percentage.

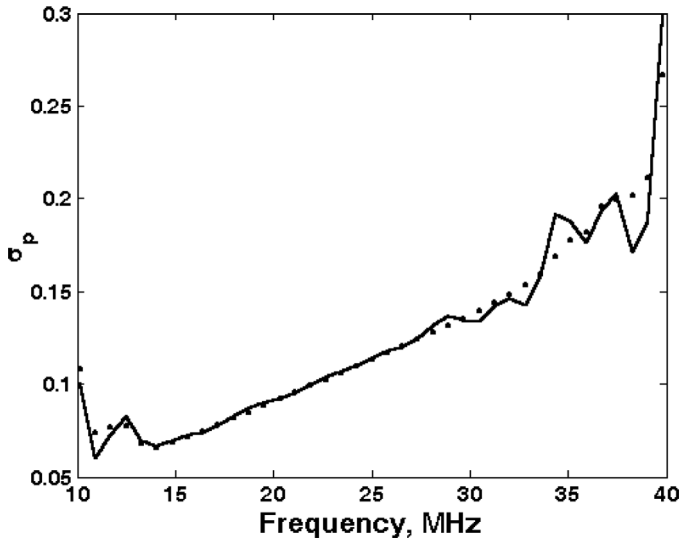

Fig. 14. Standard deviation of the phase spectrum $\sigma_p(\omega)$ expressed in radians: Experimental record (solid line), and calculated from (50) (dotted line).

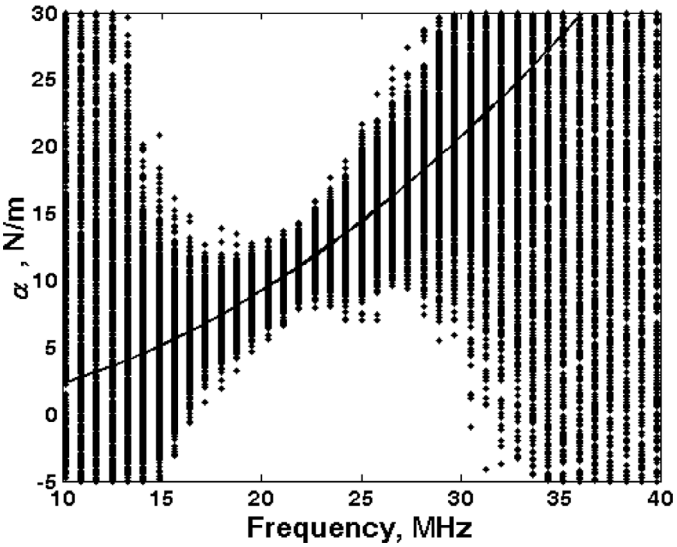

Fig. 15. Frequency domain results for water: Ensemble of measured attenuation coefficients calculated without averaging superimposed on the theoretical result (solid line). The variant nature of the experimental results is clear.

found that the standard deviation of the frame jitter was always less than 0.3 of the system sampling interval, and we believe that it is safe to take this value as a worst case estimate for all systems incorporating modern electronics.

B. Estimation of the Uncertainty of a Single Measurement

The majority of commercial ultrasonic instruments and digitizing systems are supplied with specifications that quantify the uncertainty of conventional parameters such as gain, bandwidth, and noise levels. However, we have shown above that the overall uncertainty of ultrasonic measurements depends not only on the performance of the electronic systems but also on the properties of the test medium—*viz.*, the actual attenuation that will be measured (in Nepers) over a given range of frequency. It is therefore necessary to estimate the value of this attenuation. Using the theory presented above, this is then combined with the measured or specified noise statistics to estimate the expected errors in measurement of attenuation and/or phase velocity. For example, Figs. 17 and 20 provide a clear indication of the achievable uncertainty in the case of water. The relative standard deviation of a single measurement of the attenuation coefficient was more than 10%, even close to the center of the passband of the transducer. In contrast, the same parameter for the phase velocity was less than 0.035% across a wide frequency range. The final judgment on the acceptability of a single measurement will depend on the application. Where it is necessary to detect change or no-change, the decision can be made on the basis of error bars with limit values set at, say, three standard deviations on either side of the mean. Fig. 21 gives an example of such a scheme for a single experimental record.

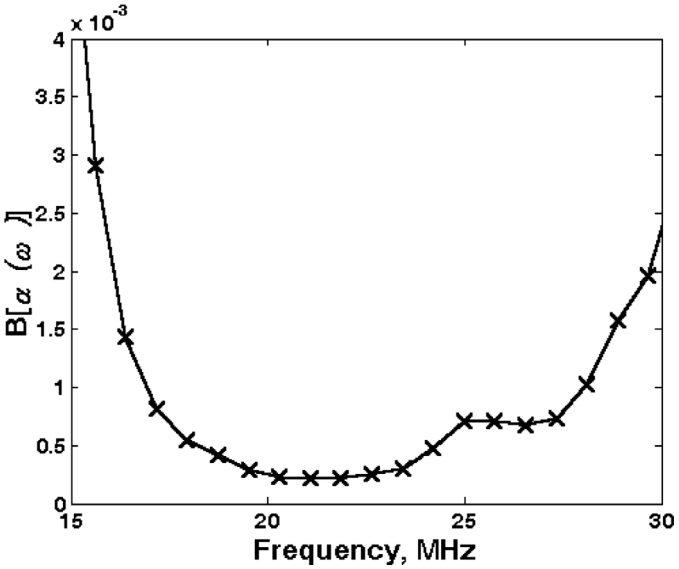

Fig. 16. Relative bias in the attenuation coefficients for water versus frequency: Values calculated using Table I (solid line), and experimental results (X's).

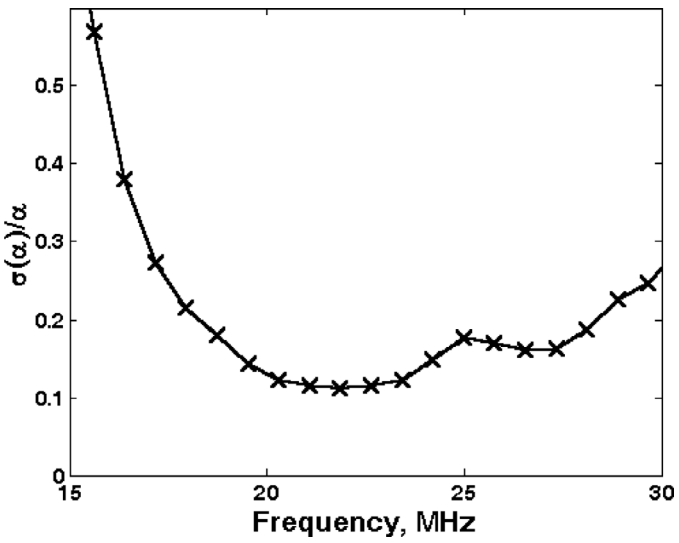

Fig. 17. Relative standard deviation of the attenuation coefficients for water versus frequency: Values calculated using Table I solid line), and experimental results (X's).

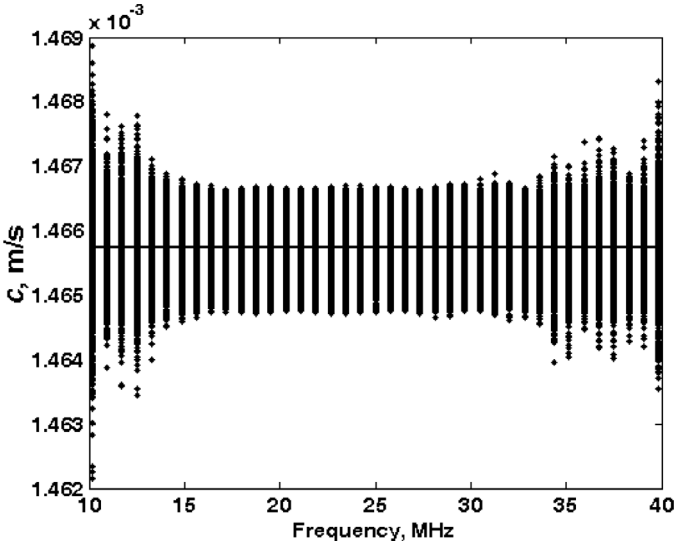

Fig. 18. Frequency domain results for water: Ensemble of measured phase velocities calculated without averaging superimposed on the theoretical group velocity (solid line).

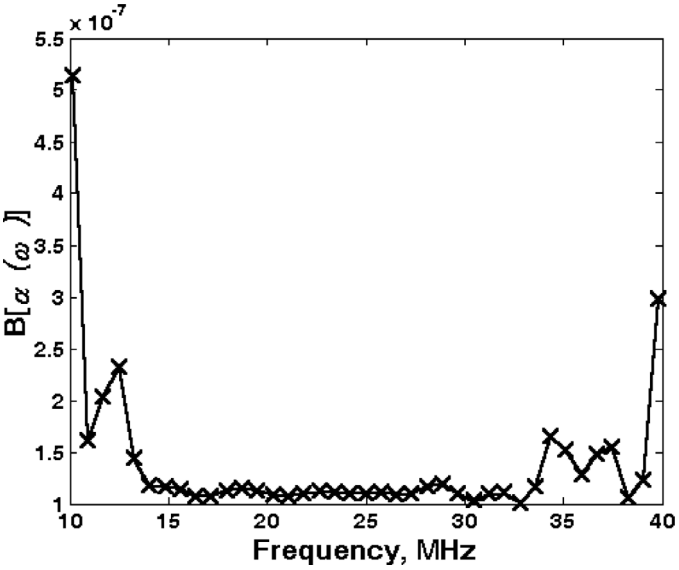

Fig. 19. Relative bias in the phase velocities for water versus frequency: Values calculated using Table I (solid line), and experimental results (X's).

C. Estimation of the Uncertainty of Measurements with Coherent Averaging

Averaging can be performed by transmitting the raw records to a personal computer, but this involves considerable time for the data transfers. Advanced instruments provide embedded averaging that reduces this overhead and speeds up measurements. However, it can still be time-consuming to assess measurement uncertainty in the conventional way by a statistical study of a large ensemble of records. In contrast, the application of (49) and (50) provide for relatively rapid estimates and incorporate the $\sqrt{L}$ reduction in the standard deviation for both the attenuation and phase velocity. For example, using $L = 100$ leads to a tenfold decrease in uncertainty; the relative standard deviation of the attenuation coefficient falls to the order of a few percent, and the standard deviation of the phase velocity to the order of 40 ppm. The corresponding graphs for change detection are shown in Fig. 22.

The required number of averages to achieve a specified uncertainty can be determined from the following expression:

$$L \geq \max\left(\sqrt{\frac{\max\left[\sigma_\alpha(\omega)\right]}{\sigma_{\alpha\ desired}}}, \sqrt{\frac{\max\left[\sigma_c(\omega)\right]}{\sigma_{c\ desired}}}\right), \quad (55)$$

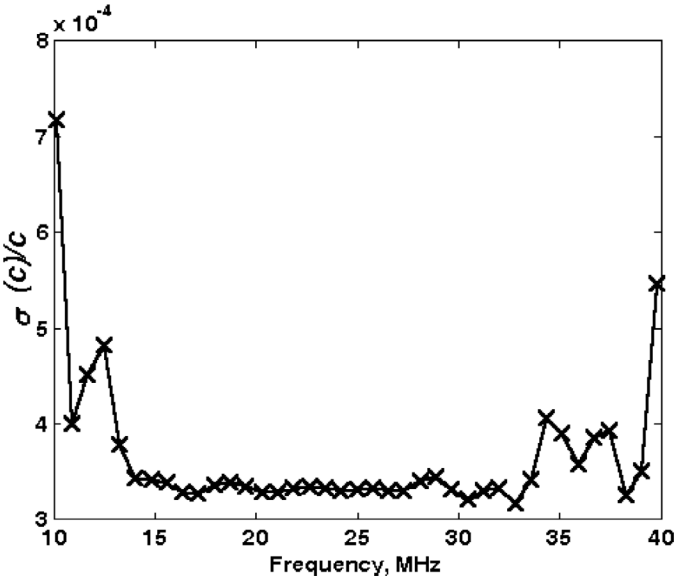

Fig. 20. Relative standard deviation of the phase velocities for water versus frequency: Values calculated using Table I (solid line), and experimental results (X's).

where the desired values for the standard deviations of the attenuation coefficient and phase velocity appear in the denominators.

D. Ultrasonic Monitoring Systems for Processes

There is growing interest in the use of ultrasonic spectrometers for monitoring chemical processes for the formation of complex liquids and polymeric materials. In these applications there are likely to be constraints on the design of both the acoustic test cell and possibly the maximum allowable signal levels that are applied to the transmitting transducer. The most significant constraint is likely to be the distance between the transmitting and receiving transducers (the gauge length d) since this will have to match plant pipe or vessel dimensions. For a given test material the total measured attenuation will be $\alpha(\omega)d$ Nepers and in most cases this will be a rising function of frequency. The transducers themselves will have a maximum response at their center frequencies, f_0, falling to close to zero near dc and at $2f_0$. The system SNR will be close to its maximum at f_0, again falling away toward dc and $2\,f_0$. The noise magnifying factors $M(\alpha(\omega)d)$ are minimum around $\alpha(\omega)d = 1$ Neper and rise rapidly for lower and higher values of $\alpha(\omega)d$. In practice, these factors limit the total measurable attenuation to lie in the range of 0.1 to 6 Nepers. For any given material with characteristic $\alpha(\omega)$ there are thus maximum and minimum limits to the frequencies at which measurements will be possible. It is useful to establish these limits *a priori* so as to avoid situations where the information required about a test material lies outside the measurable range. We therefore suggest that formal design protocols be developed for process applications; these should include experiments to estimate the range of the attenuation coefficients that are likely to be measured, and over what frequency range. Also required will be information on plant geometry to get the gauge length d, and thence the maximum and minimum total attenuations that will actually be measured. This will enable the noise magnification factor to be calculated from (17). Knowledge of the system noise standard deviation (σ_m) from (49) then permits the expected variance error in the attenuation to be calculated from (21). If this error is found to be unacceptable then a required value for σ_m can be obtained from (21) and then used in (49) and (55) to establish the number of coherent averages required to reduce noise-induced errors to acceptable levels. A decision will then be required as to whether the properties of the test material are likely to be stationary for the time required for signal averaging. Similar reasoning can be applied to the design of measurements of ultrasonic phase velocity spectra.

VI. Conclusions

Ultrasonic compression wave attenuation and phase velocity data provide useful information on the state of many complex liquid and solid materials. Errors occur in the measurement of attenuation and phase velocity, and empirical observation over many years has indicated that the range of total attenuation that was measurable fell somewhere in the range of 0.1 to 6 Nepers. This paper has presented a formal statistical approach to the sources of error and their significance. We have shown how additive electronic noise affects the uncertainty of measurements of both attenuation and phase velocity, and how timing jitter affects errors in phase velocity estimation. Our most significant observation is that electronic noise maps into measurement errors in a highly nonlinear way and gives rise to the range of measurable attenuation cited earlier in this paragraph; the optimum measurement conditions occur when the measured attenuation is close to 1 Neper.

In principle, errors can originate from digital processing of acoustic signals. However, an appropriate sampling frequency, effective anti-aliasing filters, and the use of floating point computations of adequate precision for time-to-frequency transformation render such errors negligible. The influence of the quantization process also becomes negligible if the standard deviation of the additive noise is in the order of the quantization step, and coherent averaging is employed.

Formulae have been derived that link the uncertainty of acoustical spectroscopy measurements to the statistical parameters of the instrumentation noise, timing jitter, and measurement conditions. They can be used to estimate the uncertainty of any given measurement or to establish signal processing procedures, such as coherent averaging and filtering, that would be required to achieve a specified uncertainty in any given measurement. Most significantly, the formulae provide the basis for the formal design of ultrasonic attenuation and phase velocity spectrometers.

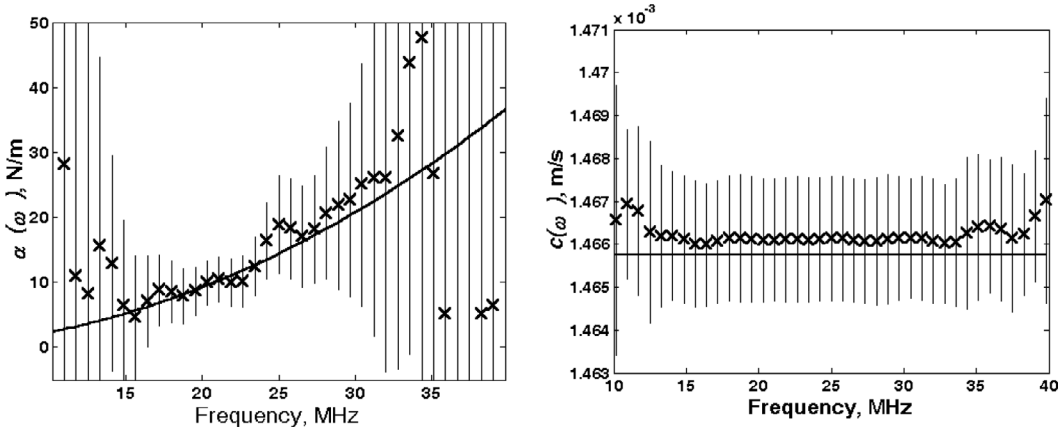

(a) (b)

Fig. 21. Attenuation coefficient (left) and phase velocity (right) for water versus frequency: Theoretical values (solid line), results for a single measurement (X's), and error bars (vertical lines).

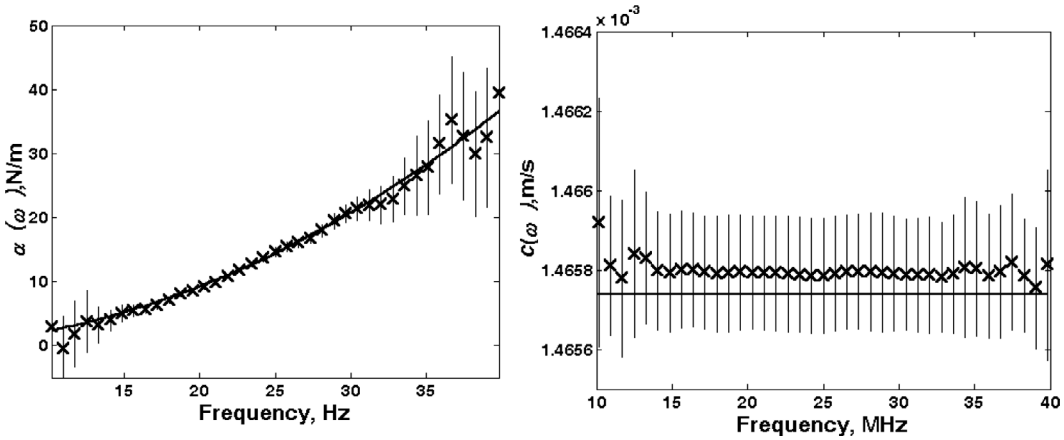

(a) (b)

Fig. 22. The effect of coherent averaging on attenuation (left) and phase velocity (right) results for water: Theoretical data (solid lines), results for a measurement incorporating 100 coherent averages (X's), and the corresponding error bars (vertical lines).

References

[1] R. E. Challis, J. A. Harrison, A. K. Holmes, and R. P. Cocker, "A wide bandwidth spectrometer for rapid ultrasonic absorption measurements in liquids," *J. Acoust. Soc. Amer.*, vol. 90, no. 2, pp. 730–740, 1991.

[2] R. E. Challis, T. Alper, A. K. Holmes, and R. P. Cocker, "Near-plane-wave acoustic propagation measurements in thin layers of adhesive polymer," *Meas. Sci. Technol.*, vol. 2, pp. 59–68, 1991.

[3] R. E. Challis, "The effect of transducer-reflector angulation on echoes received from targets using ultrasonic pulse-echo equipment," *Acustica*, vol. 50, pp. 221–225, 1982.

[4] R. E. Challis, R. J. Freemantle, R. P. Cocker, D. L. Chadwick, D. J. Dare, C. M. Martin, A. Mahendrasingam, and W. Fuller, "Ultrasonic measurements related to evolution of structure in curing epoxy resins," *Plastics, Rubber and Composites*, vol. 29, no. 3, pp. 109–118, 2000.

[5] R. J. Freemantle and R. E. Challis, "Combined compression and shear wave ultrasonic measurements on curing adhesive," *Meas. Sci. Technol.*, vol. 9, no. 8, pp. 1291–1302, 1998.

[6] R. E. Challis, J. S. Tebbutt, and A. K. Holmes, "Equivalence between three scattering formulations for ultrasonic wave propagation in particulate mixtures," *J. Phys. D: Appl. Phys.*, vol. 31, no. 24, pp. 3481–3497, 1998.

[7] D. J. Hibberd, A. K. Holmes, M. Garrood, A. Fillery-Travis, M. M. Robins, and R. E. Challis, "Ultrasonic monitoring of oil-in-water emulsions during depletion flocculation," *J. Coll. Int. Sci.*, vol. 193, pp. 77–87, 1997.

[8] T. Marshall, R. E. Challis, A. K. Holmes, and J. S. Tebbutt, "Modeling ultrasonic compression wave absorption during the seeded crystallisation of copper (II) sulphate pentahydrate from aqueous solution," *IEEE Trans. Ultrason., Ferroelect., Freq. Contr.*, vol. 49, no. 11, pp. 1583–1591, 2002.

[9] A. K. Holmes and R. E. Challis, "Ultrasonic wave propagation in sols and gels," *Langmuir*, vol. 15, pp. 3045–3049, 1999.

[10] R. E. Challis, G. P. Wilkinson, and R. J. Freemantle, "Errors and uncertainties in the pulse-echo reflectometry method for measuring acoustic impedance," *Meas. Sci. Technol.*, vol. 9, pp. 692–700, 1998.

[11] D. V. Lindley, *An Introduction to Probability and Statistics*. Cambridge, UK: Cambridge University Press, 1965.

[12] A. N. Kalashnikov, "The influence of fabrication errors on the stopband magnitude responses of SAW devices," *IEEE Trans. Ultrason., Ferroelect., Freq. Contr.*, vol. 49, pp. 475–483, Apr. 2002.

[13] A. N. Kalashnikov and R. E. Challis, "Errors in the measurement of ultrasonic absorption for material evaluation," in *Review of Progress in Quantitative Nondestructive Evaluation (28th QNDE)*. vol. 21, pp. 1997–2004, 2002.

[14] J. J. Blair, "Error estimates for frequency responses calculated from time-domain measurements," *IEEE Trans. Instrum. Meas.*, vol. IM-47, no. 2, pp. 345–353, 1998.

[15] G. Betta, C. Liguori, and A. Pietrosanto, "Propagation of uncertainty in a discrete Fourier transform algorithm," *Measurement*, vol. 27, pp. 231–239, 2000.
[16] B. Widrow, I. Kollár, and M.-C. Liu, "Statistical theory of quantization," *IEEE Trans. Instrum. Meas.*, vol. IM-45, no. 2, pp. 353–361, 1996.
[17] W. R. Bennett, "Spectra of quantized signals," *Bell Syst. Tech. J.*, vol. 27, pp. 446–472, July 1948.
[18] R. M. Gray, "Quantisation noise spectra," *IEEE Trans. Inform. Theory*, vol. IT-36, no. 6, pp. 1220–1244, 1990.
[19] M. K. Brown, "On quantization of noisy signals," *IEEE Trans. Signal Processing*, vol. SP-39, no. 4, pp. 836–841, 1991.
[20] J. Schoukens and J. Renneboog, "Modelling the noise influence on the Fourier coefficients after a discrete Fourier transform," *IEEE Trans. Instrum. Meas.*, vol. IM-35, no. 3, pp. 278–286, 1986.
[21] O. Meste and H. Rix, "Jitter statistics estimation in alignment processes," *Signal Processing*, vol. 51, pp. 41–53, 1996.
[22] D. A. Skoog, F. J. Holler, and T. A. Nieman, *Principles of Instrumental Analysis*. London: Thomson Learning, 1998, ch. 13.
[23] A. N. Kalashnikov and R. E. Challis, "Errors in the measurement of ultrasonic phase velocity in the context of materials evaluation," in *Review of Progress in Quantitative Nondestructive Evaluation (29th QNDE)*. vol. 22B, pp. 1227–1234, 2003.
[24] A. N. Kalashnikov, R. E. Challis, M. E. Unwin, and A. K. Holmes, "Quantification of frame jitter in data acquisition systems," in *Proc. 2003 IEEE Int. Symp. Intelligent Signal Process.*, Budapest, 4–6 Sep. 2003, pp. 15–20.

Alexander N. Kalashnikov was born in 1962 in Odessa, Ukraine. He graduated in electrical engineering from Odessa State Polytechnic University (OSPU, Odessa, Ukraine) in 1984. He obtained his candidate of science degree by thesis on surface acoustic wave devices from Odessa State Academy of Telecommunications (Odessa, Ukraine) in 1991, and his doctor of science degree from OSPU in 1999. Between 1984 and 1999 he worked at OSPU as an engineer, junior researcher, Ph.D. student, lecturer, senior lecturer, associate professor, postdoctoral researcher, and finally chief researcher. He came to the United Kingdom as a research associate at Loughborough University in 1999, and in 2000 joined the School of Electrical and Electronic Engineering at the University of Nottingham as a lecturer. He is a member of IEEE and the American Mathematical Society, and was awarded a Senior Researcher qualification by the Ukraine Supreme Qualification Committee (1997).

Richard E. Challis was born in 1945 in the United Kingdom. He received the B.Sc. (Eng) and Ph.D. degrees in 1967 and 1975, respectively, in electrical engineering from the Imperial College of Science, Technology and Medicine, London. He has worked in the electrical engineering industry and in the health service in the United Kingdom. He was Professor of Engineering Physics at the University of Keele, UK and subsequently Head of the School of Electrical and Electronic Engineering at the University of Nottingham, UK. Dr. Challis' principal area of research is instrumentation for industrial manufacturing and processes, with particular emphasis on quality assurance techniques for adhered metal assemblies and for colloidal materials in process. He is a Fellow of the Institution of Electrical Engineers, a Fellow of the Institute of Physics, and a Fellow of the British Institute of Non-Destructive Testing. He was elected a Fellow of the Royal Academy of Engineering in 2004.